Nano Res (2010) 3: 363–368
DOI 10.1007/s12274-010-1040-2
Research Article

Surface Active Sites on Co_3O_4 Nanobelt and Nanocube Model Catalysts for CO Oxidation

Linhua Hu, Keqiang Sun, Qing Peng, Boqing Xu, and Yadong Li (✉)

Department of Chemistry, Tsinghua University, Beijing 100084, China

Received: 13 January 2010 / Revised: 15 February 2010 / Accepted: 20 March 2010
© The Author(s) 2010. This article is published with open access at Springerlink.com

ABSTRACT

CO oxidation has been performed on Co_3O_4 nanobelts and nanocubes as model catalysts. The Co_3O_4 nanobelts which have a predominance of exposed {011} planes are more active than Co_3O_4 nanocubes with exposed {001} planes. Temperature programmed reduction of CO shows that Co_3O_4 nanobelts have stronger reducing properties than Co_3O_4 nanocubes. The essence of shape and crystal plane effect is revealed by the fact that turnover frequency of Co^{3+} sites of {011} planes on Co_3O_4 nanobelts is far higher than that of {001} planes on Co_3O_4 nanocubes.

KEYWORDS

CO oxidation, Co_3O_4, surface active sites, turnover frequency, model catalyst

1. Introduction

CO oxidation is an important probe reaction in the development of many novel catalytic materials and catalytic mechanisms. A gold catalyst for CO oxidation below 0 ˚C was first reported by Haruta et al. in 1987 [1]. The size effect for such gold catalysts was verified by Goodman et al. in 2002 using a model catalyst of a gold cluster supported on a single crystalline surface of TiO_2 {110} [2]. The shape effect for CeO_2 nanocrystals in CO oxidation was reported by our group in 2005, when we showed that nanorods with exposed {110} planes prepared by a hydrothermal method are more reactive than nanoparticles with exposed {100} and {111} planes prepared by a precipitation method [3]. Si et al. subsequently prepared Au–CeO_2 nanocomposite catalysts with different shapes of CeO_2 crystals and found a similar crystal plane effect for the water–gas shift reaction [4]. Observation of such unexpected properties usually results from employing special techniques in the fabrication of catalytic materials [5, 6].

Co_3O_4, a typical spinel-structure transition metal oxide, has attracted considerable attention for CO oxidation, and is regarded as an alternative to gold catalysts [7–10]. In 2008, our group [11] developed a hydrothermal method using cobalt hydroxide as a precursor and subsequent direct thermal decomposition to obtain Co_3O_4 nanobelts with exposed {011} planes, nanosheets with exposed {112} planes, and nanocubes with exposed {001} planes. The unusually high index {112} crystal planes of Co_3O_4 nanocrystals are more reactive than the more common {001} and {011} planes in the catalytic combustion of methane [11]. Xie et al. subsequently prepared Co_3O_4 nanorods by a similar method which showed better catalytic properties than Co_3O_4 nanoparticles for CO oxidation at

Address correspondence to ydli@mail.tsinghua.edu.cn

temperatures as low as –77 ˚C; this can be attributed to the abundance of active Co^{3+} species on {110} planes in the former, assuming that the turnover frequencies (TOF) of the Co^{3+} sites are approximately the same level for the nanorods and the nanoparticles [12]. However, the shape of the nanoparticles they used for comparison is a truncated octahedron exposing {001} and {111} planes, so that the estimated TOF is an average result for {001} and {111} planes. Therefore, nanocubes with only {001} planes exposed are more suitable for investigating shape effects on CO oxidation. The Co^{3+} ions of Co_3O_4 are the active sites for CO oxidation and Co^{2+} ions are almost inactive [8, 13]. From the viewpoint of traditional heterogeneous catalysts, the catalytic activity of a material depends on the number surface active sites. The relationship between the shape/crystal plane effect and the surface active sites is therefore a very important link between the structures and properties of catalysts.

In this work, we prepare Co_3O_4 nanobelts and nanocubes according to Ref. [11] and investigate their behavior as model catalysts for CO oxidation. We show that the TOF of the Co^{3+} sites on Co_3O_4 nanobelts is significantly higher than that of Co^{3+} sites on Co_3O_4 nanocubes.

2. Experimental

2.1 Catalyst preparation

Co_3O_4 nanocubes and Co_3O_4 nanobelts were prepared via a hydrothermal process using a cobalt hydroxide precursor and subsequent direct thermal decomposition [11].

2.1.1 Nanocubes

$Co(NO_3)_2{\cdot}6H_2O$ (1 mmol, 0.291 g) was dissolved in 20 mL of ethanol to form a red solution, and then a mixture of 2 mL of octadecenylamine and 10 mL of ethanol was added to the solution with magnetic stirring for at least 30 min. The resulting green solution was transferred into a 40-mL autoclave with a Teflon liner and heated at 180 ˚C for 12 h. The resulting product was filtered and washed several times with cyclohexane and ethanol, dried under vacuum at 60 ˚C for 2 h, and finally calcined in air at 350 ˚C for 3 h.

2.1.2 Nanobelts

$Co(NO_3)_2{\cdot}6H_2O$ (1 mmol, 0.291 g) was dissolved in 15 mL of H_2O to form a red solution, and then 20 mL glycerol was added to the solution with magnetic stirring for at least 30 min. The resulting solution was transferred into a 40-mL autoclave with a Teflon liner and heated at 140 ˚C for 12 h. The resulting $Co(CO_3)_{0.5}(OH){\cdot}0.11H_2O$ nanobelts were calcined in air at 350 ˚C for 3 h to produce Co_3O_4 nanobelts.

2.2 Catalyst characterization

Powder X-ray diffraction (XRD) patterns were obtained by using a Bruker D8 Advance X-ray diffractometer with Cu Kα radiation (λ = 1.5418 Å). The size and morphology of all the catalysts were examined with a JEOL JEM-1200EX transmission electron microscope (TEM) and a Tecnai TF20 high-resolution transmission electron microscope (HRTEM). The catalyst powders were dispersed in ethanol to prepare samples for TEM and HRTEM. The BET surface area of the catalysts was measured by N_2 adsorption using the multi-point method.

CO temperature-programmed reduction (CO-TPR) experiments were performed using a Thermo Electron Corporation TPD/R/O 1100 Series Catalytic Surfaces Analyzer equipped with an AMETEK quadrupole mass spectrometer which allowed detection of the various reaction products. In the CO-TPR experiments, a gas mixture of CO (5 vol% in He, 20 mL/min) was flowed over the sample (50 mg) [pre-treated with O_2 (10 vol% in He, 20 mL/min) at 300 ˚C for 30 min] with heating from room temperature to 800 ˚C at a rate of 10 ˚C/min.

2.3 Catalytic activity

The catalytic activities for CO oxidation were evaluated in a fixed-bed quartz tubular reactor (6 mm i.d., 300 mm long) at atmospheric pressure under steady-state conditions. The catalyst particles (0.2 g) were placed in the reactor to a height of ca. 4 mm. The reactant gases (2.5% CO, 20% O_2, balanced with nitrogen) were passed through the reactor at a rate of 100 mL/min with a contact time of 2×10^{-5} h. The CO oxidation reaction was stabilized for 15 min, and the outlet products were then measured by gas chromatography. In every case, carbon dioxide was the only reaction

product detected throughout the whole experiment.

3. Result and discussion

3.1 Catalyst characterization

Figure 1 shows typical scanning electron microscope (SEM), TEM, and HRTEM images of the Co_3O_4 nanobelts and nanocubes. The lengths and widths of the Co_3O_4 nanobelts are ca. 2–5 μm and 50–100 nm, respectively, while the as-prepared Co_3O_4 nanocubes are monodisperse with a uniform size of ca.15–20 nm. The average length and width of the nanobelts are 3.5 μm and 75 nm, respectively. The average length of the nanocubes is ca. 17.5 nm. The dominant exposed planes of Co_3O_4 nanobelts are {011}, which are the only planes normal to both the set of (311) planes with a lattice spacing of 0.24 nm and the set of (222) planes with a crossing lattice spacing of 0.23 nm. The dominant exposed planes of Co_3O_4 nanocubes are

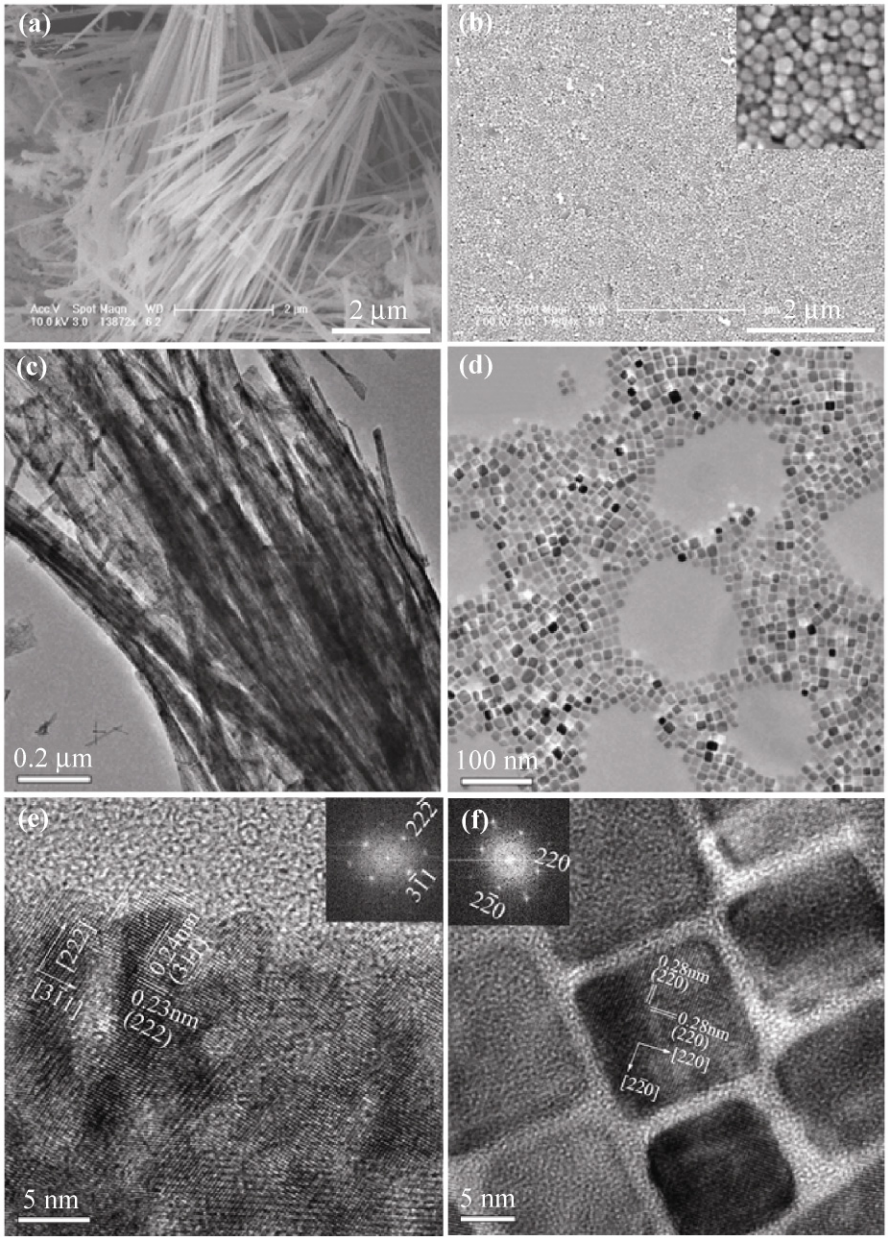

Figure 1 (a) SEM image of typical Co_3O_4 nanobelts. (b) SEM image of typical Co_3O_4 nanocubes. (c) TEM image of typical Co_3O_4 nanobelts. (d) TEM image of typical Co_3O_4 nanocubes. (e) HRTEM image of a typical nanobelt and (f) HRTEM image of a typical nanocube

{001}, which are the only planes normal to the set of (220) planes with a lattice spacing of 0.28 nm.

The XRD patterns (Fig. S-1 in the Electronic Supplementary Material (ESM)) show that Co_3O_4 nanobelts and nanocubes can be indexed as the fcc phase (space group $Fd\bar{3}m$) with a lattice constant a = 8.065 Å, which is consistent with the values in the literature (JCPDS# 74-1657).

For the nanobelts, the estimated crystal size of the thickness (h) normal to the {011} surface is ca. 17.3 nm according to Scherrer equation. Therefore, the calculated surface area of the nanobelts is ca. 23.6 $m^2 \cdot g^{-1}$, which is close to the experimental BET surface area of 20.1 $m^2 \cdot g^{-1}$. For the nanocubes, the estimated crystal size of the thickness (h) normal to the {001} surface is ca. 21 nm according to the Scherrer equation, which is consistent with the size of 20 nm given by HRTEM. The calculated surface area of the nanocubes is 56.5 $m^2 \cdot g^{-1}$, which is higher than the experimental BET surface area of 22.6 $m^2 \cdot g^{-1}$. These results indicate that the nanocubes are probably aggregated, and that there is almost no influence of the cracks and interspaces within the nanobelts.

3.2 Catalytic activity

Figure 2 shows the catalytic properties of differently shaped Co_3O_4 nanocrystals. For a gas hourly space velocity (GHSV) of 50 000 h^{-1}, the values of T_{10} (the temperature which gives a 10% CO conversion) for Co_3O_4 nanocubes and nanobelts are 61 ℃ and 56 ℃, respectively. The CO conversion is 10% over Co_3O_4 nanobelts and 7% over Co_3O_4 nanocubes at 56 ℃, with the corresponding mass specific rates of conversion of CO being 0.85 and 0.62 μmol·g^{-1}·s^{-1}, respectively, as shown in Table 1. The specific rate of conversion over Co_3O_4 nanobelts at 56 ℃ is therefore 1.37 times higher than that over the nanocubes, indicting that the Co_3O_4 nanobelts are significantly more active than Co_3O_4 nanocubes. At 56 ℃, the TOF of Co^{3+} sites on the nanobelts is 7.4×10^{-3} s^{-1}, whilst it is only 2.7×10^{-3} s^{-1} for the nanocubes, indicating that the TOF of Co^{3+} sites on {011} planes is 2.7 times higher than those on {001} planes. Details of the calculations of the TOF values are given in the ESM. The Co^{3+} sites on the nanobelts are far more reactive than those at the nanocubes. No deactivation was observed when the Co_3O_4 nanocubes and nanobelts were reused in a second run.

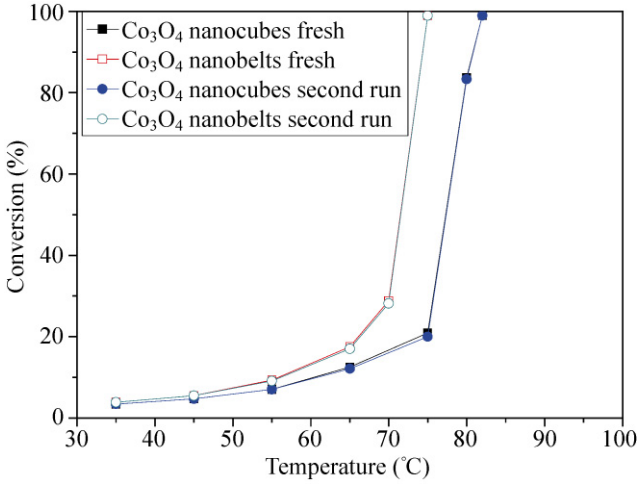

Figure 2 CO conversion as a function of reaction temperature over Co_3O_4 nanobelts and nanocubes at GHSV = 50 000 h^{-1} (reactants are oxygen and CO)

Table 1 Catalytic properties of Co_3O_4 nanobelts and nanocubes

T_{10} (℃)	Reaction rate (μmol·g^{-1}·s^{-1})		TOF (s^{-1})	
	Nanobelts	Nanocubes	Nanobelts	Nanocubes
56	0.85	0.62	7.4×10^{-3}	2.7×10^{-3}

The TOF of the nanoparticles might be an overestimate since the calculations assume that the only active sites are those exposed at the corners and edges of spherical particles with 5%–10% defects [12]. In fact, there are six equivalent {001} planes on nanocubes without defects which expose the first sub-layer of Co^{3+} sites to reactant oxygen and CO. The different locations of Co^{3+} sites on {011} and {001} planes are expected to lead to a difference in catalytic activity. The active Co^{3+} sites in the nanobelts are located on the surface layer of the {011} planes as shown in Figs. 3(a) and 3(b), whereas those in the nanocubes are on the first sub-layer of the {001} plane with a distance of 1.008 Å to the topmost surface layer as shown in Figs. 3(c) and 3(d). In the presence of CO and O_2, CO is adsorbed on the Co^{3+} sites of Co_3O_4, and surface lattice oxygen is transferred from Co^{2+} to Co^{3+} leading to the production of CO_2, and the resulting oxygen vacancy is subsquently filled by reaction with O_2 [14]. The adsorption of CO on the first sub-layer of Co^{3+} sites is expected to be more

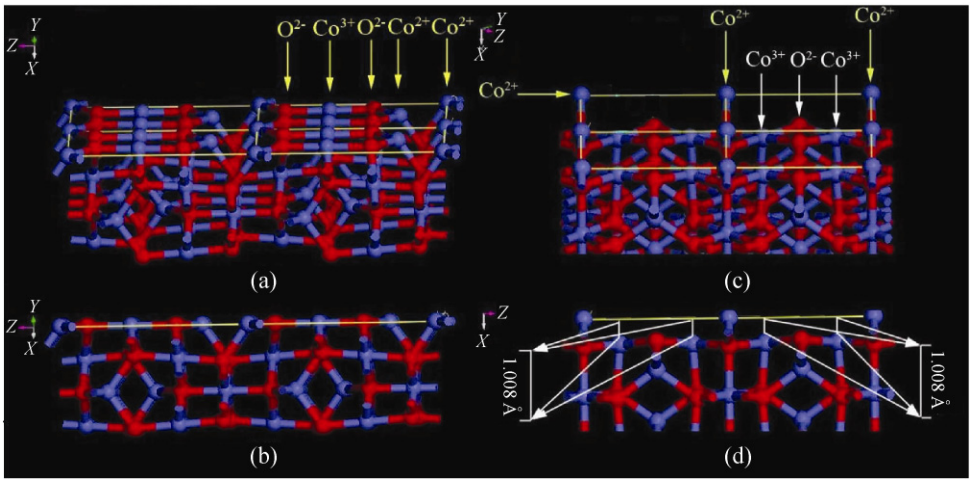

Figure 3 (a) Surface atoms of the Co_3O_4 {011} plane. (b) Horizontal view of the Co_3O_4 {011} plane. (c) Surface atoms of the Co_3O_4 {001} plane. (d) Horizontal view of the Co_3O_4 {001} plane. Atoms highlighted with yellow arrows are located on the surface layer of the plane, and those with white arrows on the first sub-layer of the plane

diffcult than on the topmost surface layer of Co^{3+} sites, which is consistent with the relative catalytic activities of the nanobelts and nanocubes. Therefore, the location of Co^{3+} sites on different planes is the major influence on the catalytic activity to CO.

Figure 4 compares the CO-TPR profiles of Co_3O_4 nanobelts and nanocubes obtained by simultaneously monitoring the signals of CO consumption and CO_2 formation by mass spectroscopy. For Co_3O_4 nanobelts, the broader peak centered at 290 ℃ and the narrower peak centered at 343 ℃ can be attributed to the reduction of Co^{3+} to Co^{2+} (step Ⅰ) and Co^{2+} to Co^0 (step Ⅱ) [15, 16], respectively. For the reduction of the Co_3O_4 cubes, the corresponding peaks shift to 301 ℃ and 365 ℃, respectively. This indicates that the Co_3O_4 nanobelts show a higher reducibility than their nanocube counterparts. Surface lattice oxygen is regarded as playing an important role in the reduction reactions [17, 18]. For the nanobelts, there is only one kind of surface layer lattice oxygen in the {011} planes which has a coordination number of three (one Co^{2+}–O^{2-} and two Co^{3+}–O^{2-}) bonds. For the nanocubes, the first sub-layer lattice oxygen in the {001} planes has the three same bonds in its coordination shell. In the absence of gaseous oxygen, the reduction requires breaking of the lattice oxygen bonds and subsquent reaction with CO. The surface layer lattice oxygen is more easily activated by CO than the first sub-layer

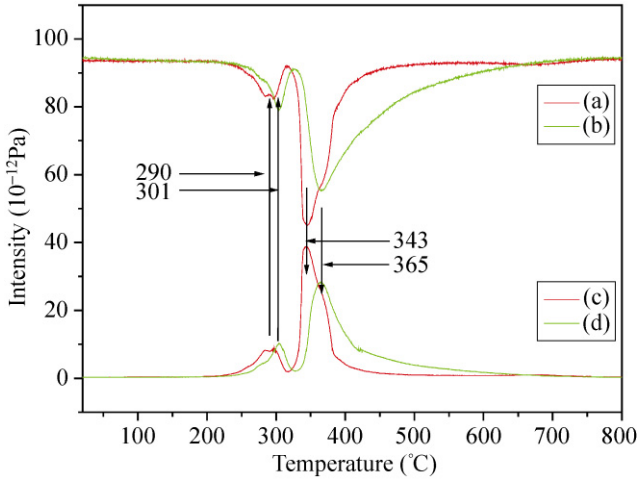

Figure 4 CO-TPR profiles of Co_3O_4 nanocrystals. (a) and (b) are the traces of the CO consumption signals for the Co_3O_4 nanobelts and nanocubes, respectively. (c) and (d) are the traces of the CO_2 formation signals for the Co_3O_4 nanobelts and nanocubes, respectively

lattice oxygen, which is a possible reason for the stronger reducing properties of {011} planes compared with {001} planes.

4. Conclusions

CO oxidation has been performed on Co_3O_4 nanobelts exposing primarily {011} planes and nanocubes exposing primarily {001} planes. The {011} planes show a higher catalytic activity for CO oxidation than the

{001} planes. The importance of shape and crystal plane effects is highlighted by the fact that the Co^{3+} sites on {011} planes are more reactive than those on {001} planes. These findings are of importance in the development of shape-controllable nanocrystal model catalysts and provide guidance for practical heterogeneous catalysis.

Acknowledgements

This work was supported by National Natural Science Foundation of China (NSFC) (Nos. 10979031, 20921001, and 90606006), the "973" State Key Project (No. 2006CB932303), and the China Postdoctoral Science Foundation (No. 20080440361).

Electronic Supplementary Material: XRD patterns of Co_3O_4 nanobelts and nanocubes, together with details of the calculations of surface areas and TOF values are available in the online version of this article at http: //dx.doi.org/10.1007/s12274-010-1040-2 and accessible free of charge.

Open Access: This article is distributed under the terms of the Creative Commons Attribution Noncommercial License which permits any noncommercial use, distribution, and reproduction in any medium, provided the original author(s) and source are credited.

References

[1] Haruta, M.; Kobayashi, T.; Yamada, N. Novel gold catalysts for the oxidation of carbon monoxide at a temperature far below 0 °C. *Chem. Lett.* **1987**, *16*, 405–408.

[2] Valden, M.; Lai, X.; Goodman, D. W. Onset of catalytic activity of gold clusters on titania with the appearance of nonmetallic properties. *Science* **1998**, *281*, 1647–1650.

[3] Zhou, K. B.; Wang, X.; Sun, X. M.; Peng, Q.; Li, Y. D. Enhanced catalytic activity of ceria nanorods from well-defined reactive crystal planes. *J. Catal.* **2005**, *229*, 206–212.

[4] Si, R.; Flytzani-Stephanopoulos, M. Shape and crystal-plane effects of nanoscale ceria on the activity of Au–CeO_2 catalysts for the water–gas shift reaction. *Angew. Chem. Int. Ed.* **2008**, *47,* 2884–2887.

[5] Wang, X.; Zhuang, J.; Peng, Q.; Li, Y. D. A general strategy for nanocrystal synthesis. *Nature* **2005**, *437*, 121–124.

[6] Wang, D. S.; Xie, T.; Li, Y. D. Nanocrystals: Solution-based synthesis and applications as nanocatalysts. *Nano Res.* **2009**, *2*, 30–46.

[7] Huang, X. S.; Sun, H.; Wang, L. C.; Liu, Y. M.; Fan, K. N.; Cao, Y. Morphology effects of nanoscale ceria on the activity of Au/CeO_2 catalysts for low-temperature CO oxidation. *Appl. Catal. B* **2009**, *90*, 224–232.

[8] Jansson, J.; Palmqvist, A. E. C.; Fridell, E.; Skoglundh, M.; Österlund, L.; Thormählen, P.; Langer, V. On the catalytic activity of Co_3O_4 in low-temperature CO oxidation. *J. Catal.* **2002**, *211*, 387–397.

[9] Luo, J. Y.; Meng, M.; Li, X.; Li, X. G.; Zha, Y. Q.; Hu, T. D.; Xie, Y. N.; Zhang, J. Mesoporous Co_3O_4–CeO_2 and Pd/Co_3O_4–CeO_2 catalysts: Synthesis, characterization and mechanistic study of their catalytic properties for low-temperature CO oxidation. *J. Catal.* **2008**, *254*, 310–324.

[10] Tüysüz, H.; Comotti, M.; Schüth, F. Ordered mesoporous Co_3O_4 as highly active catalyst for low temperature CO-oxidation. *Chem. Commun.* **2008**, 4022–4024.

[11] Hu, L. H.; Peng, Q.; Li, Y. D. Selective synthesis of Co_3O_4 nanocrystal with different shape and crystal plane effect on catalytic property for methane combustion. *J. Am. Chem. Soc.* **2008**, *130*, 16136–16137.

[12] Xie, X. W.; Li, Y.; Liu, Z. Q.; Haruta, M.; Shen, W. J. Low-temperature oxidation of CO catalysed by Co_3O_4 nanorods. *Nature*, **2009**, *458*, 746–749.

[13] Petitto, S. C.; Marsh, E. M.; Carson, G. A.; Langell, M. A. C. Cobalt oxide surface chemistry: The interaction of CoO(1 0 0), Co_3O_4(1 1 0) and Co_3O_4(1 1 1) with oxygen and water. *J. Mol. Catal. A* **2008**, *281*, 49–58.

[14] Yu, Y. B.; Takei, T.; Ohashi, H.; He, H.; Zhang, X. L.; Haruta, M. Pretreatments of Co_3O_4 atmoderate temperature for CO oxidation at –80 °C. *J. Catal*. **2009**, *267*, 121–128.

[15] Liotta, L. F.; Carlo, G. D.; Pantaleo, G.; Deganello, G. Co_3O_4/CeO_2 and Co_3O_4/CeO_2–ZrO_2 composite catalysts for methane combustion: Correlation between morphology reduction properties and catalytic activity. *Catal. Commun.* **2005**, *6*, 329–336.

[16] Van't Blik, H. F. J.; Prins, R. Characterization of supported cobalt and cobalt–rhodium catalysts: I. Temperature-programmed reduction (TPR) and oxidation (TPO) of Co–Rh/Al_2O_3. *J. Catal*. **1986**, *97*, 188–199.

[17] Yaremchenko, A. A.; Kharton, V. V.; Veniaminov, S. A.; Belyaev, V. D.; Sobyanin, V. A.; Marques, F. M. B. Methane oxidation by lattice oxygen of $CeNbO_{4+\sigma}$. *Catal. Commun.* **2007**, *8*, 335–339.

[18] Bossche, M. V. D.; McIntosh, S. The rate and selectivity of methane oxidation over $La_{0.75}Sr_{0.25}Cr_xMn_{1-x}O_{3-\delta}$ as a function of lattice oxygen stoichiometry under solid oxide fuel cell anode conditions. *J. Catal*. **2008**, *255*, 313–323.